

Effect of pore geometry on Gassmann fluid substitution

Fuyong Yan* and De-Hua Han

Rock Physics Laboratory, University of Houston

Received October 2014, revision accepted October 2015

ABSTRACT

Although there is no assumption of pore geometry in derivation of Gassmann's equation, the pore geometry is in close relation with hygroscopic water content and pore fluid communication between the micropores and the macropores. The hygroscopic water content in common reservoir rocks is small, and its effect on elastic properties is ignored in the Gassmann theory. However, the volume of hygroscopic water can be significant in shaly rocks or rocks made of fine particles; therefore, its effect on the elastic properties may be important. If the pore fluids in micropores cannot reach pressure equilibrium with the macropore system, assumption of the Gassmann theory is violated. Therefore, due to pore structure complexity, there may be a significant part of the pore fluids that do not satisfy the assumption of the Gassmann theory. We recommend that this part of pore fluids be accounted for within the solid rock frame and effective porosity be used in Gassmann's equation for fluid substitution. Integrated study of ultrasonic laboratory measurement data, petrographic data, mercury injection capillary pressure data, and nuclear magnetic resonance T_2 data confirms rationality of using effective porosity for Gassmann fluid substitution. The effective porosity for Gassmann's equation should be frequency dependent. Knowing the pore geometry, if an empirical correlation between frequency and the threshold pore-throat radius or nuclear magnetic resonance T_2 could be set up, Gassmann's equation can be applicable to data measured at different frequencies. Without information of the pore geometry, the irreducible water saturation can be used to estimate the effective porosity.

Key words: Rock physics, Fluid substitution, Specific surface area, Effective porosity.

INTRODUCTION

With improvement of seismic data quality and processing techniques, quantitative seismic attribute analysis for direct hydrocarbon indication is becoming practical and widely applied. Gassmann fluid substitution is one of the most important tools to model the seismic attribute responses of the reservoir rocks due to different pore fluids. Gassmann theory is well studied because of its importance in seismic exploration (Smith, Sondergeld, and Rai 2003). Skelt (2004) studied Gassmann fluid substitution in laminated sands. Dvorkin, Mavko, and Guverich (2007) studied the application of

Gassmann's equations in shaly sediments. Mavko and Bandyopadhyay (2009) brought up an approximate formulation of fluid substitution for vertical velocities in weakly anisotropic vertically transversely isotropic (VTI) rocks. Sil, Sen, and Gurevich (2011) studied fluid substitution in a porous and fractured medium. The Gassmann theory is extended to two- or multiple-phase porous media (Berryman and Milton 1991; Carcione *et al.* 2005). It is even generalized for solid substitution (Ciz and Shapiro 2007; Grechka 2009; Saxena and Mavko 2014).

Our study is focused on application of the classical Gassmann theory. Sarout (2012) studied the impact of pore space topology on permeability, cut-off frequencies, and validity of wave propagation theories. Although there is no pore

*E-mail: yanfyon@yahoo.com

geometry assumption in the Gassmann theory on elasticity of porous media, one of the most important assumptions is that the pore fluids reach pressure equilibrium in a representative volume (Gurevich *et al.* 2009). This assumption is not always satisfied for seismic wave propagation in reservoir rocks. Pores have different sizes and shapes, and the pore walls are made of different minerals; thus, the pore fluids may respond quite differently to a minor pressure disturbance. The typical strain in non-destructive ultrasonic measurement is in the order of 10^{-9} (Rose 1999), which means the pressure disturbance is in the order of tens of Pascals for common reservoir rock. The pressure disturbance is in the order of several hundreds of Pascals for seismic wave propagating in reservoir rocks if the strain is assumed less than 10^{-8} . Depending on the distance to the pore walls, the surface tension on pore fluids may be so strong that some portion of the pore fluids does not move like the normal pore fluid under the influence of the passing pressure waves. For example, it may need stress of 1 GPa to move the hygroscopic water away from the mineral surface (Plaster 2008). The pore throats for some pores (mostly micropores) may be too narrow for their effective communication with the macropore system (Mavko and Jizba 1991). Thus, to apply Gassmann fluid substitution, the porosity should be apparent or effective porosity, which is the volume fraction of pore fluid that is connected and relaxed, and the other fraction of the pore fluid should be included in the rock frame material. Under this principle, we can invert the fraction of effective porosity from laboratory-measured data. Comparing the inverted result with the pore geometry information derived from petrographic images, mercury injection capillary pressure (MICP) and nuclear magnetic resonance (NMR) T_2 data, we can have better understanding of importance of the pore geometry and its influence on the pore fluid saturation effect predicted by the Gassmann theory.

Pore geometry and pore fluid mobility

The pore geometry that we discuss here primarily refers to the pore size distribution and the specific surface area. The pore size can have variation of several orders from less than one nanometre to several millimetres. Specific surface area (S_s) is defined as the interstitial surface area of the pores and pore channels per unit of bulk volume, per unit of grain volume, per unit of pore volume, or per unit of weight of a material (Salem and Chilingarian 1999). It can be measured by physical absorption of gas using the Brunauer–Emmett–Teller (BET) theory (Brunauer, Emmett, and Teller 1938). The specific surface area is primarily controlled by the pore size. If we assume that the pore system consists of N identical oblate

Table 1 Specific surface area of some clay minerals (after Corey 1986)

Clay type	S_s , m ² /gram
Kaolinite	45
Illite	175
Montmorillonite	800

spheroidal pores with pore aspect ratio (α) far less than 1, then the specific surface area can be approximated by

$$S_s = \frac{N2\pi R^2}{N\frac{4}{3}\pi\alpha R^3} = \frac{3}{2\alpha R}, \quad (1)$$

where R is the pore radius and α is the pore aspect ratio. Let the pore radius R be 100 nm and α be 0.01, then 1 cm³ volume of such a pore system can have a surface area of 1,500 m². If there are four layers of water molecules covering this area, the water will take up all the pore volume (the diameter of water molecule is about 0.29 nm). Obviously, the pore aspect ratio and roughness of the pore wall can also have significant effect on specific surface area. For reservoir rocks, the large surface area is primarily related to clay minerals. Table 1 shows the specific surface area values for some common clay minerals.

Specific surface area has close relation with two important parameters for reservoir engineers: irreducible water saturation (S_{wir}) and permeability, which determine the petroleum recovery factor and efficiency, respectively. It is usually believed that the irreducible water saturation is closely related to porosity: The lower is the porosity, the higher the irreducible water saturation. As shown in Fig. 1, when S_{wir} is plotted against porosity, no obvious trend can be observed, but when it is plotted against S_s , the trend is clear. This is because most of the minerals in the reservoir rock can adsorb water; the bigger the S_s , the more water will be adhered to the pore wall surfaces. Permeability is often cross-plotted with porosity because they are correlated. In Fig. 2(a), there is a general trend that the permeability increases with porosity, but the data points are quite scattered. When permeability is plotted against ϕ/S_s , the correlation is significantly improved. The strong correlation illustrates that permeability is primarily controlled by porosity and S_s , but they have opposite effects on permeability: More pore space is favorable for fluid movement, but bigger specific surface area will resist fluid movement.

Several mechanisms of water adsorption on mineral surface have been proposed by Low (1961). They include hydrogen bonding, hydration of exchange cations, attraction by osmosis, charged surface–dipole attraction, attraction by London dispersion forces, and capillary condensation. Figure 3 shows schematically the moisture tension around a

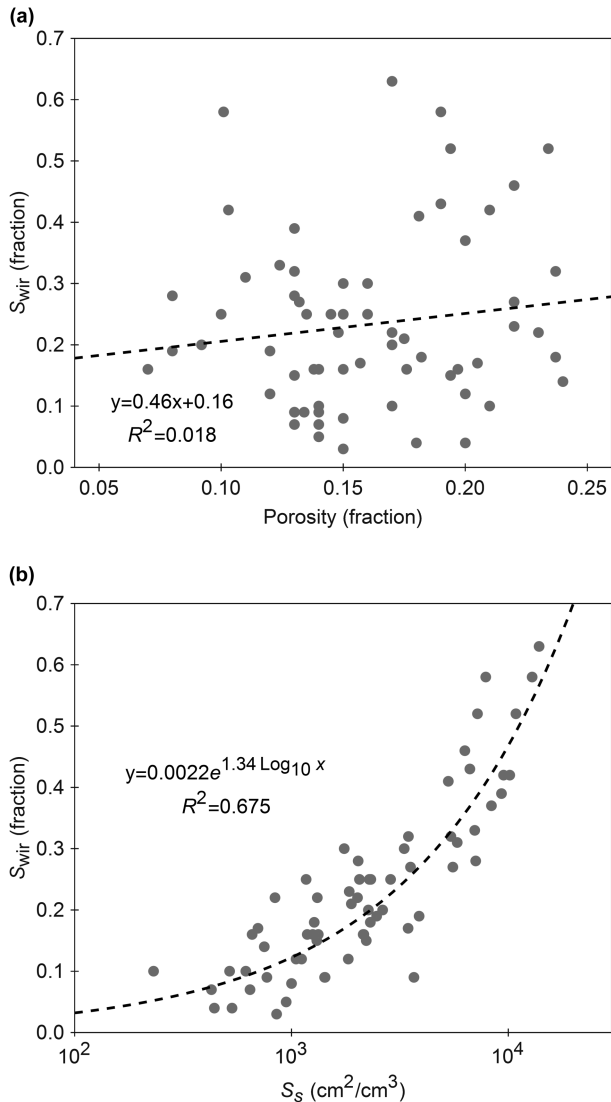


Figure 1 Comparing crossplots between S_{wir} versus total porosity and S_{wir} versus specific surface area. The specific surface area here defined as pore surface area per unit of pore volume. (Data from Bagrintseva 1977; Chilingarian, Chang, and Bagrintseva 1990).

soil particle. Soil is a mixture of unconsolidated minerals, water, air, and organic matter, and can have similar mineral composition to the reservoir rocks. The soil-moisture tension is the force per unit area required to remove the film water from soil. In Fig. 3, depending on the distance of the water molecule to the mineral surface, the attraction between the mineral surface and the water molecule can be far greater than the pressure disturbance caused by seismic waves in seismic exploration, which means part of the fluid will behave more like rigid rock frame material than the normal pore fluid. The hygroscopic

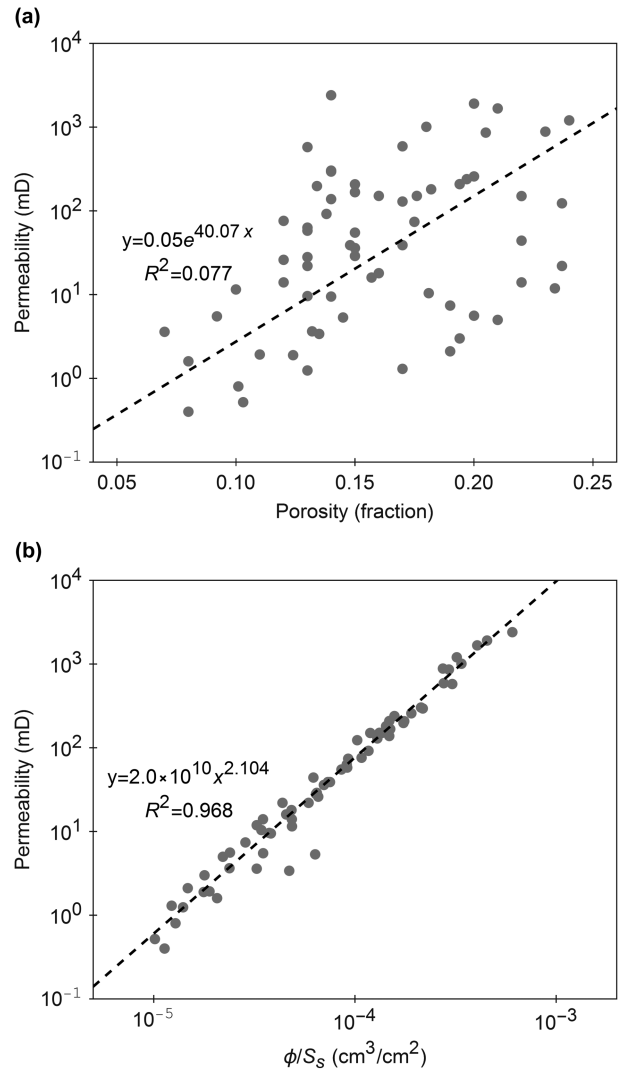


Figure 2 Comparison of crossplots between permeability versus total porosity and permeability versus ϕ/S_s (Data from Bagrintseva 1977; Chilingarian *et al.* 1990).

water is part of the pore fluids that most tightly bond on the mineral surfaces. It can be as thick as 10–20 layers of water molecules. For fine-grained particles, the maximum weight content of hygroscopic water may reach 0.9% in quartz, 8%–17% in feldspars, and 36%–48% in micas (Pinneker 2010).

Effective porosity for Gassmann fluid substitution

The most important contribution of the Gassmann theory is to describe the effect of pore fluids on the elastic properties of the porous medium. The Gassmann's equations are often written

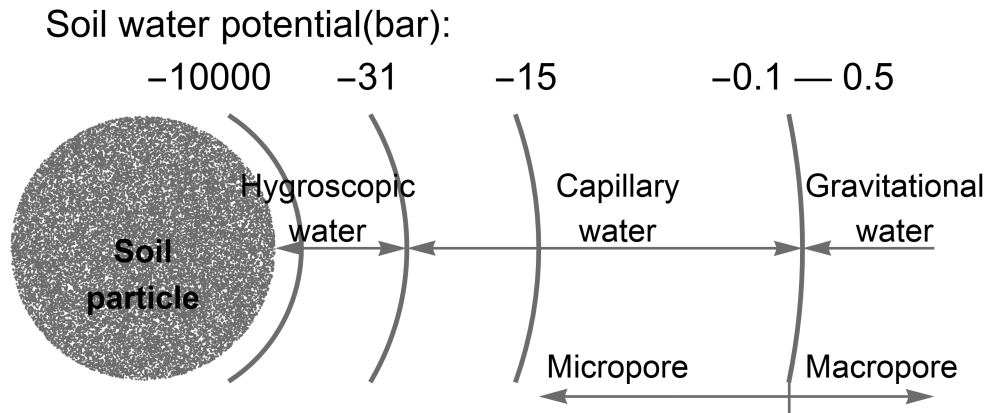


Figure 3 Soil moisture tension around soil particles. Here, the negative sign means that force(stress) are needed to take water away from the surface of the soil particle. Positive sign means water will flow downward under influence of gravity (modified after Plaster 2008).

in the following form (Gassmann 1951; Mavko, Mukerji, and Dvorkin 1998):

$$\frac{K_{sat}}{K_m - K_{sat}} = \frac{K_{dry}}{K_m - K_{dry}} + \frac{K_f}{\phi(K_m - K_f)}, \quad (2)$$

$$\mu_{sat} = \mu_{dry}, \quad (3)$$

where K_{sat} is the bulk modulus of the rock filled with pore fluid, K_m is the bulk modulus of the solid rock frame, K_{dry} is the bulk modulus of the dry rock, K_f is the bulk modulus of the pore fluid, and ϕ is porosity. μ_{sat} and μ_{dry} are the shear moduli of the fully saturated and dry rocks, respectively. It is noted that equation (3) is a conclusion and not an assumption of the Gassmann theory (Berryman 1999). Because equation (3) is straightforward and simple in form, Gassmann's equation for isotropic porous medium is often referred to equation (2) only.

Several explicit assumptions are made in derivation of Gassmann's equation (Gassmann 1951). They include (a) macroscopically homogeneous and isotropic porous medium, (b) differential elasticity, (c) connected pore system, and (d) frictionless pore fluids. Assumption (a) is obvious. Assumption (b) is important because most of the reservoir rocks are not perfectly elastic, but under very small stress disturbance (tens to hundreds of Pascals), the reservoir rocks can be approximated as elastic. Theoretically, assumption (c) is not a necessary condition as shown by Grechka (2009). For a porous medium whose pores are disconnected but have identical shape, the pressure disturbances in each pore are equal during passing of the elastic waves. Therefore, Gassmann's equation still stands. This can be directly proved by the Kuster–Toksöz's theory (Kuster and Toksöz 1974). The significance of assumption (d) is sometimes overlooked. The fric-

tionless fluid is an ideal fluid that has zero viscosity; therefore, the pore fluids in different pore shapes (e.g., neighboring crack and stiff pore) can reach pressure equilibrium instantly. For reservoir rocks filled with frictionless fluid, there should be no dispersion and attenuation caused by the squirt flow (or the dispersion occurs at infinite high frequency), and there is also no dispersion caused by the Biot flow. In this case, the Gassmann theory is frequency independent and works as long as the pore system is connected. In practice, the reservoir fluids are not frictionless, the pore fluids in the cracks of reservoir rocks do not satisfy the assumption of Gassmann's equations, and this part of pore fluids should be accounted for within the frame material. For consolidated reservoir rocks, the effect of the Biot flow is usually not significant and occurs at around ultrasonic frequency; thus, we can still assume Gassmann's equations work, but we primarily consider the saturation effect of the pore fluids in the macropore system.

In his paper, Gassmann (1951) also discussed effect of hygroscopic water. He pointed out that elasticity of the skeleton may change through accumulation of hygroscopic water on the pore walls. The hygroscopic water distinguishes itself from the normal pore fluid through its larger density, higher pressure, and smaller mobility. Usually, the volume of hygroscopic water is negligibly small. Our discussion in the previous section shows that the volume of hygroscopic water can be significant for rocks with very large specific surface area. The rocks with larger specific surface area generally have smaller mean grain size (Salem and Chilingarian 1999). Researches also show strong correlation between hygroscopic water and clay contents (Banin and Amiel 1970; Petersen *et al.* 1996; Resurreccion *et al.* 2011; Wuddivira *et al.* 2012). Thus, for fine-grained rocks or rocks with high clay content, the

hygroscopic water should be treated separately from normal pore fluids when Gassmann's equation is applied for fluid substitution.

When Gassmann (1951) brought up the theory, he also used a numerical example to illustrate how to apply his theory. In the numerical example, the sandstone has a total porosity of 17.1%. The dry rock is immersed in water. However, part of the pores is inaccessible to the water; therefore, the apparent porosity is 13.3%. To apply his theory, he suggested that the apparent porosity should be used in equation (2), and the "inaccessible" pores should be "accounted for within the solid material" (Gassmann 1951 and Berryman *et al.* 2007). Therefore, when Gassmann brought up his theory, he realized the pores should not necessarily be treated equally and as a whole entity.

In laboratory measurement, it is often not straightforward to evaluate the dryness of the core samples. Even the lunar dry rock contains minute amount of water (Robinson and Taylor 2014). King, Marsden, and Dennis (2000) studied the Biot dispersion of seismic wave velocities in partially and fully saturated sandstones with small clay content. He suggested that the elastic properties of the "dry" sandstone are determined after the dry sandstone initially adsorbs small amounts of moisture. By doing so, part of the pore fluids is actually treated as the solid frame material. Therefore, selection of the "dry" state is closely related to determination of effective porosity to be used in Gassmann's equation.

Dvorkin *et al.* (2007) applied the concept of dual porosity on shaly sediments. They estimate the effective porosity that should be used for Gassmann fluid substitution by

$$\phi_e = \phi_t - \phi_{clay}C, \quad (4)$$

where ϕ_t is the total porosity, C is the clay content, and ϕ_{clay} is the intrinsic porosity of clay minerals. The concept of intrinsic porosity of clay may be geologically improper. The porosity of the clay content varies with types of the clay minerals, compaction, diagenesis, etc. For example, using the technique of back-scattered electron microscopy, Nadeau and Hurst (1991) estimated from shaly sandstone samples that the microporosity of kaolinite is 15%–61%, the microporosity of chlorite is 44%–58%, and the microporosity of illite is 47%–76%. It is not necessarily true that all pores associated with clay minerals are ineffective (Luney *et al.* 2001).

The pore space occupied by the hygroscopic water or isolated from the macropore system should not be accounted in the effective porosity for Gassmann's equation. The complex pore system can be modelled by pore aspect ratio spectrum (Cheng 1978; Yan *et al.* 2014). Depending on the frequency

of the elastic wave and pore aspect ratio, the pore fluids in soft pores may not be able to reach pressure equilibrium with the macropore system in a representative volume; thus, this part of pores should not be accounted in the effective porosity for Gassmann's equation as well. For generality, we define all the pores that can reach pressure equilibrium in a representative volume to be effective pores for Gassmann's equation, and the others pores are ineffective. Obviously, the effective porosity is frequency dependent and can change slightly with frequency. All the pore fluids in the ineffective pores are accounted in the rock frame material, and its effective moduli are estimated using Voigt–Reuss–Hill (VRH) averaging scheme (Smith 2003). The "modified" Gassmann's equation is in the same form as the original Gassmann's equation:

$$\frac{K_{sat}}{K'_m - K_{sat}} = \frac{K'_{dry}}{K'_m - K'_{dry}} + \frac{K_f}{\phi_e(K'_m - K_f)}, \quad (5)$$

where K'_m is the effective bulk modulus of the rock matrix, including pore fluids in ineffective pores, and K'_{dry} is the pseudo dry bulk modulus for partially saturated rock with ineffective pores filled with pore fluids. K'_{dry} can be measured in the laboratory. The word "modified" is quoted because it is not a real modification. In the numerical example in his paper, Gassmann (1951) applied his own theory in this way. The Gassmann theory is the low-frequency-limit case of the Biot theory. In practical application, the acoustic data upon which Gassmann's equation applied are often acquired at a frequency range violating the low frequency assumption. By treating part of the pore fluids as part of the solid rock frame, the dispersion effect is also considered; therefore, Gassmann's equation can be applicable to acoustic data of various frequencies.

The pseudo dry bulk modulus is usually not measured in laboratory because it is very difficult to control how much and which parts of pores are filled with pore fluids. Irreducible water saturation quantifies the pore fluids that cannot be driven out by mechanic force; thus, it might be proper to approximate the effective porosity using the following formula if we do not have reliable information of the dynamic effective porosity:

$$\phi_e \approx \phi_t (1 - S_{wir}). \quad (6)$$

The effective bulk modulus at this saturation state is approximated as a pseudo dry bulk modulus. Figure 4 shows the ultrasonic measurement of the partial saturation effect of a loose sandstone sample from the Gulf of Mexico. The gas is injected into the sample fully saturated with water. The lowest water saturation point is where the injected gas cannot

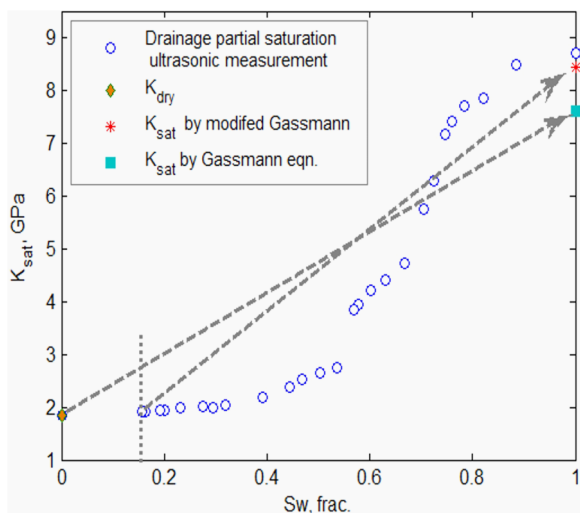


Figure 4 Comparison of saturation effect prediction by Gassmann’s equation using total porosity and effective porosity (The core sample is a loose sandstone from Gulf of Mexico, with $\phi = 34.79\%$, $S_{wir} = 0.156$).

further reduce the water saturation of the rock sample, and it is approximated as the irreducible water saturation. Here, we only consider three saturation states: dry, irreducible water saturation, and 100% water saturation. We use equations (2) and (5), respectively, to predict the effective bulk modulus of 100% brine-saturated rock and compare them with the measured value. The predicted effective bulk modulus using Gassmann’s equation with effective porosity is much closer to the measured value than using the total porosity. Therefore, the “modified” Gassmann’s equation can better predict the saturation effect on the seismic wave velocity.

For practical application of fluid substitution using the logging data, we do not need to estimate the pseudo dry bulk modulus and can use the equation below for fluid substitution:

$$\frac{K_{sat1}}{K'_m - K_{sat1}} - \frac{K_{f1}}{\phi_e (K'_m - K_{f1})} = \frac{K_{sat2}}{K'_m - K_{sat2}} - \frac{K_{f2}}{\phi_e (K'_m - K_{f2})}, \tag{7}$$

where subscripts 1 and 2 represent different pore fluid saturation conditions. The critical step in applying equation (7) is to estimate the effective porosity from logging data or other sources.

Inversion of effective porosity from laboratory measurement

In laboratory ultrasonic velocity measurements, core samples are commonly measured on both room-dry and fully

saturated conditions. Petrographic data of the core samples can supply us information about the mineral composition and pore structure. If we could invert the effective porosity using the ultrasonic measurement data and compare the results with the petrographic data, it may help us have better understanding of the relationship between the pore geometry and the saturation effect on seismic velocities.

For consolidated rock, Han (1986) showed that the Biot dispersion is usually much smaller than the dispersion induced by interaction between pore fluids in soft pores and stiff pores (s squirt flow). By applying fluid substitution using effective porosity as described in equation (5), the dispersion caused by the squirt flow is actually considered and included in K'_m . Therefore, we can assume the Gassmann theory works on ultrasonic measurement data and use equation (5) to invert the effective porosity. The pseudo K_{dry} is not measured, and we can use the following equation to approximate it:

$$K'_{dry} = \frac{1}{2} \left[\left(\frac{\phi_t - \phi_e}{\phi_t} \right) K'_M + \frac{\phi_e}{\phi_t} K_{dry} + \frac{K'_M K_{dry}}{\frac{\phi_e}{\phi_t} K'_M + \left(\frac{\phi_t - \phi_e}{\phi_t} \right) K_{dry}} \right]. \tag{8}$$

The pseudo K_{dry} is approximated by the VRH average of the real K_{dry} and K'_M . K'_M is the effective bulk modulus of the rock matrix, including pore fluids in ineffective pores. Conceptually, all the pore fluids in the ineffective pores are moved to one side so that one part of the rock is fully saturated and the other part is completely dry. The volume fraction of the fully saturated section is $(\phi_t - \phi_e)/\phi_t$, and the effective bulk modulus is K'_M ; the volume fraction of the completely dry section is ϕ_e/ϕ_t , and the effective bulk modulus is K_{dry} . By substituting equation (8) into equation (5), the only unknown parameter is ϕ_e ; thus, it can be calculated.

Figure 5 shows the inverted fraction of effective porosity relative to the total porosity using Han’s data (Han 1986), and the ultrasonic measurement data on core samples from a tight gas reservoir. The core samples with clay content higher than 10% are not included because there might be significant non-mechanical effect during drying/saturating of the shaly sandstone (Vanorio, Scotellaro, and Mavko 2007; Baechle *et al.* 2009; Yan and Han 2011). From the inversion result, the fraction of effective porosity generally increases with total porosity. This is expected since the effective pores are usually macropores whose volume can be drastically reduced by diagenesis. The pore filling cementation minerals (clay minerals, calcite, and quartz) not only decrease the porosity, increase the tortuosity, and narrow the pore throat but can also increase the specific surface area (Neasham 1977; Panda and Lake

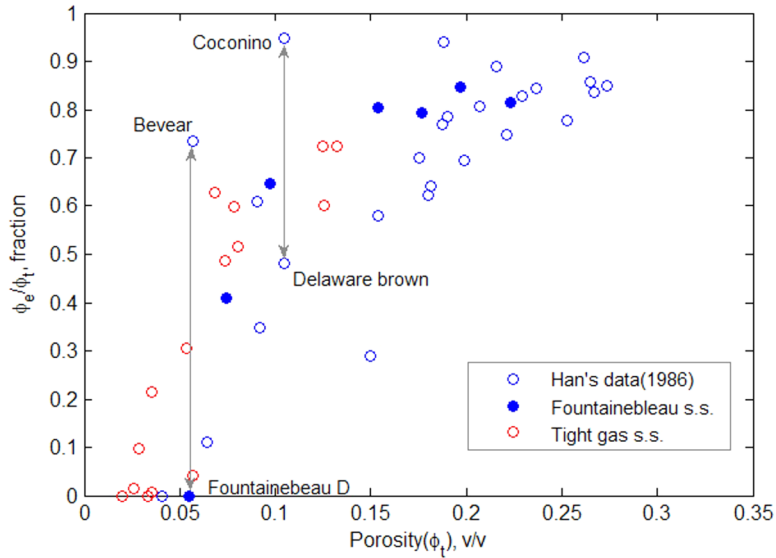


Figure 5 Inverted fraction of effective porosity relative to the total porosity. The Fontainebleau sandstones are also from Han's data (1986). The double arrows denote a sample pair with similar total porosity but very different fraction of effective porosity. Their thin section images are shown in the next figure. All the core samples have clay content less than 10%.

1995; Davis *et al.* 2006; Cook, Goodwin, and Boutt 2011). Based on automated imaging analysis and imaging processing techniques, Dillon *et al.* (2004) simulated the effect of diagenesis on evolution of sandstone porosity and found that the macroporosity decreases with compaction and the specific surface area increases compaction. Therefore, the total porosity generally decreases with diagenesis, and with reduction of the total porosity, the volume fraction of the effective porosity decreases.

Although there is a general trend of decreasing fraction of effective porosity with decreasing total porosity as shown in Fig. 5, the data points are fairly scattered. Two pairs of core samples with similar porosity are marked by up and down arrows. The Beaver sandstone has similar (slightly higher) porosity as the Fontainebleau D sandstone, but the former has about 75% of pore spaces that are effective, whereas there are almost no effective pores in the Fontainebleau D sandstone. This can be explained by comparing their thin section images (Fig. 6). The original inter-granular pores in Fontainebleau D sandstone are almost completely filled by the overgrowth of quartz; there are no macropores found under optical microscope, whereas the inter-granular macropores are well kept for the Beaver sandstone. Similar is true for the Coconino sandstone and the Delaware brown sandstone. The Coconino sandstone is from a thick cross-bedded eolian deposit acting as an important regional aquifer (Weisman 1984); its inter-granular macropores are kept much better than the Delaware brown sandstone. There is one low outlier with total porosity of 15.9%. We do not have the petrographic data of this sample. It has the highest clay content (10%) allowed in the

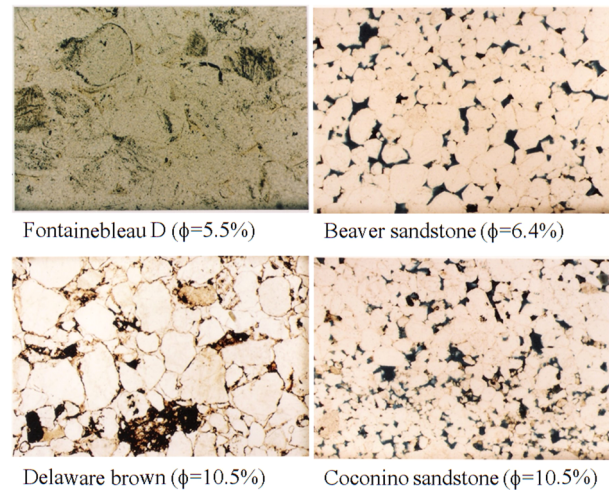
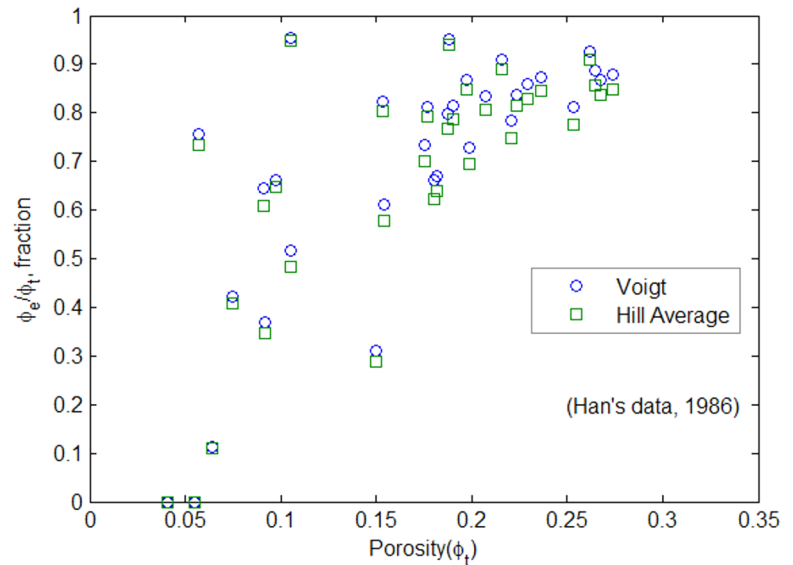


Figure 6 Thin sections under plane polarized light. Except of Fontainebleau D representing an area of $0.9 \times 1.3 \text{ mm}^2$, the other three thin sections represent actual area of $2.2 \times 3.2 \text{ mm}^2$ (Yale 1984; Velasco 1986). Pores are identified by dark areas with low relief.

dataset for inversion. The low abnormality may be related to the relatively high clay content.

In the above analysis, the pseudo-dry bulk modulus is approximated by the VRH average. There are a lot of effective medium models that can be used to estimate the pseudo K_{dry} . Obviously, different effective porosity will be inverted if different models are used. In choosing a proper model to approximate the pseudo K_{dry} , we need to consider both rationality and simplicity. A more complicated model may involve parameters that are often not available in practical

Figure 7 Comparison of the inverted fractions of effective porosity relative to the total porosity by using the Hill average (equation (8)) and the Voigt bound (equation (9)), respectively, to approximate pseudo K_{dry} . The average difference is 0.023.



application. To test the sensitivity on model selection, we compare the inverted effective porosities using the VRH average (also called Hill average) and the Voigt bound, respectively, based on Han’s data (1986). The pseudo K_{dry} can be approximated by the Voigt bound as

$$K'_{dry} = \left(\frac{\phi_t - \phi_e}{\phi_t} \right) K'_M + \frac{\phi_e}{\phi_t} K_{dry}. \tag{9}$$

Figure 7 shows the comparison of the inverted effective porosities using the VRH average (equation (8)) and the Voigt bound (equation (9)). It can be seen that the difference is generally not significant. The average difference is about 0.02 in fraction of effective porosity relative to the total porosity. The VRH average and the Voigt bound are considered effective medium models with significant difference. Therefore, the inversion results are not sensitive to selection of effective medium model to approximate the pseudo K_{dry} .

It is noticed in Fig. 4 that the difference between pseudo K_{dry} and real K_{dry} is almost negligible. In Fig. 5, generally, if the total porosity is big, the ineffective porosity will be small, and as a result, the volume of the pore fluids in ineffective pores is usually very small relative to the volume of the solid frame material. Therefore, it will not make significant difference between K_m and K'_m by including a very small portion of pore fluids in the solid frame material. From above analysis, the difference in the saturation effects predicted by Gassmann’s equation and the “modified” Gassmann are primarily determined by how much porosity is used for fluid substitution. It

can also be explained by the simplified Gassmann’s equation (Han and Batzle 2004):

$$K_{sat} \approx K_{dry} + G(\phi) K_f, \tag{10}$$

where $G(\phi)$ is the gain function defined by

$$G(\phi) = \frac{(1 - K_{dry}/K_M)^2}{\phi}. \tag{11}$$

Because the difference between pseudo K_{dry} and real K_{dry} , and the difference between K_m and K'_m are small, the saturation effect is primarily controlled by the porosity used for fluid substitution: The smaller the porosity, the greater the saturation effect.

From above analysis, the pore fluids in the micropores should usually not be included in Gassmann fluid substitution. The validity of the Gassmann theory for reservoir rocks depends on the pore structure or pore geometry. Next, we will use MICP data and NMR data to study the effect of pore geometry on Gassmann fluid substitution.

PORE GEOMETRY FROM MICP

Mercury injection capillary pressure (MICP) data are one of the most commonly acquired data for reservoir evaluation. It can supply information about core porosity, pore geometry, recovery efficiency, and permeability of the reservoir rocks (Wardlaw and McKellar 1981; Owolabi and Watson 1993; Leal *et al.* 2001). Neasham (1977) classified dispersed clay in sandstone in three categories: (a) discrete particles;

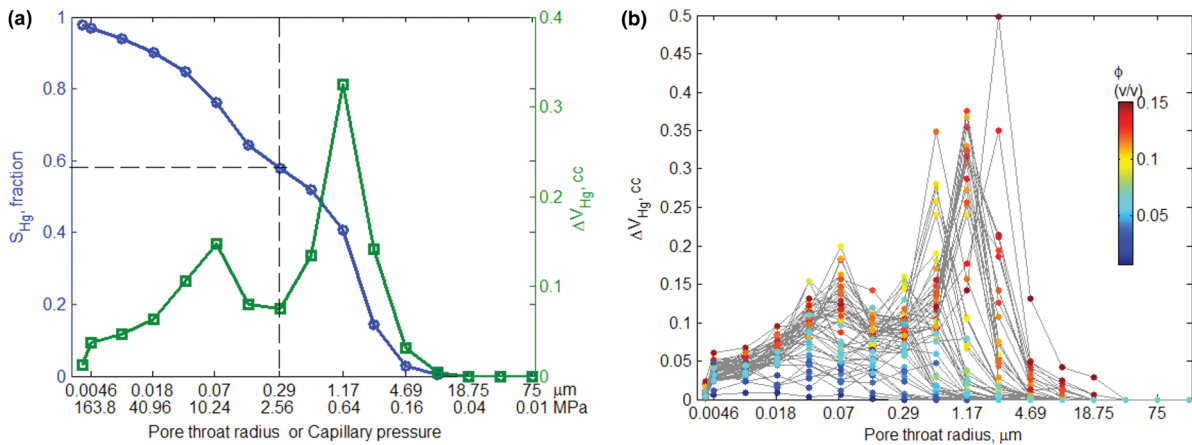


Figure 8 Mercury injection data from a tight gas sandstone reservoir. (a) Derivation of pore-throat size distribution from mercury injection data. (b) Pore throat distribution of 54 core samples from a tight gas reservoir.

(b) inter-grown crystal linings on pore walls; and (c) crystals bridging across pores. He noticed that the capillary injection curves have distinct differences for these three categories of clay content in sandstones. Therefore, MICP data can be an important source for the pore geometry study.

Derivation of pore-throat size distribution from MICP data was first brought up by Washburn (1921). With advancing of the technology, the mercury can be injected into pore throat with a diameter of several nanometres. Mercury is a non-wetting fluid for common minerals in the reservoir rocks. The pore-throat size under certain pressure (capillary pressure) being broken through by mercury is calculated by

$$r_c = \frac{2 \sigma \cos \theta}{P_c}, \quad (12)$$

where σ is the interfacial tension of mercury on minerals, the value of 0.480 N/m is often used, and the contact angle θ for mercury on minerals is often taken as 140° (Tiab and Donaldson 2004).

Figure 8(a) shows an example of deriving pore-throat size distribution from mercury injection data of one core sample. Driven by step-increasing pressure, mercury preferably enters pores connected by wider pore throat. At each step, the volume of mercury entered is recorded. The maximum mercury injection pressure applied is 200 MPa, which corresponds to pore-throat radius of 3.8 nm. Normalized by the total pore volume, the distribution of the pore-throat sizes connecting different pore volumes can be derived.

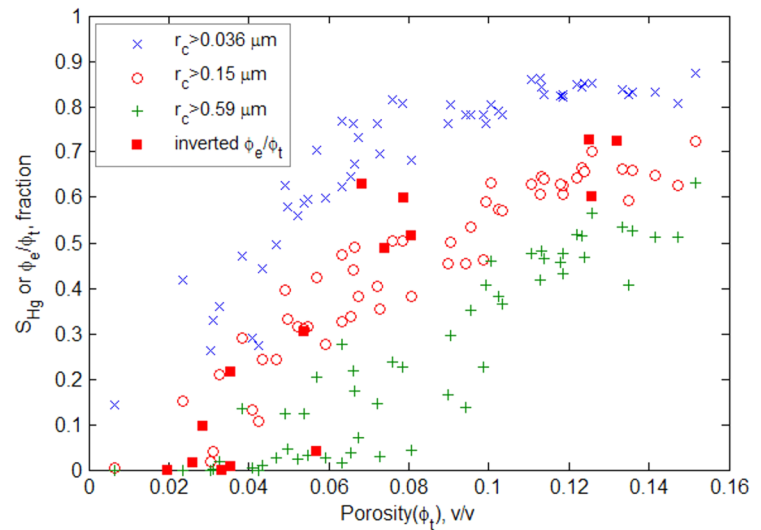
Figure 8(b) shows the pore-throat radius distribution for 54 core samples from a tight gas sandstone reservoir. During the mercury injection test, the pressure increasing steps are same for all the core samples, and the corresponding

pore-throat sizes determined by equation (12) are not dependent on the samples tested if the basic lithology of the samples is similar. At each pressure increase, the amount of mercury injected might be different; thus, different shapes of curves in Fig. 8 represent different pore geometries. In Fig. 8, for this tight gas reservoir, generally, the better quality reservoir rocks (porosity higher than 8%) has a dual-porosity structure, and the pore spaces of the poor quality rocks (porosity lower than 8%) are mostly contributed by micropores. The good reservoir rocks originally have worse sorting and lower porosity; thus, there is less water movement in geological time, and the macropores are well kept. The poor reservoir rocks originally have better sorting and higher porosity, but chemical deposition from the water movements in geological time fills most of the inter-granular macropores.

ESTIMATION OF THRESHOLD PORE-THROAT RADIUS

We also have made ultrasonic velocity measurement on 16 core samples from this tight gas sandstone reservoir, under both dry and saturated conditions. Using the methodology introduced earlier we can invert the effective porosity from the laboratory measurement (Fig. 9). The relationship between the pore size and pore-throat size is complicated and very difficult to be quantitatively studied. Good to poor correlations exist between the pore size and pore-throat size for different reservoir rocks (Wardlaw, Li, and Forbes 1987; Lindquist *et al.* 2000). Generally, the pore throat with bigger size connects bigger pores, and the pore throat with smaller size can connect both small and big pores. For macropores connected by thin cracks, the pore-throat size is primarily determined by

Figure 9 Estimation of threshold pore-throat radius by matching effective porosity from MICP data (Fig. 8) and those inverted from ultrasonic measurement using “modified” Gassmann’s equation. The effective porosity for MICP is simply estimated by trying different threshold pore-throat sizes. The estimated threshold pore-throat radius (r_c) is about $0.15 \mu\text{m}$.



the wideness or aspect ratio of the crack, so that it can be very small compare with the connected macropores. Despite the complicated relationship between pore-throat size and pore size, usually smaller pore-throat sizes are corresponding to more specific surface area, more absorbed fluid on pore walls, and more difficulty in reaching pore pressure equilibrium between the crack and the macro pore system. Therefore, we can assume that there is a threshold pore-throat radius and that all pore spaces connected with pore throat wider than this threshold are effective and the other pores are ineffective for Gassmann fluid substitution.

By trying different threshold pore-throat radii corresponding to different mercury injection pressures and matching the trends of fractional effective porosity with that inverted from the ultrasonic measurement, we can estimate threshold pore-throat radius. In Fig. 9, if we assume that only pores connected by a pore throat with a radius wider than $0.036 \mu\text{m}$ are effective; obviously, it is an overestimation of the effective porosity. If we assume only pores connected by a pore throat with radius wider than $0.59 \mu\text{m}$ are effective, obviously, it is an underestimation of the effective porosity. The best match is achieved when threshold pore-throat radius of $0.15 \mu\text{m}$ is selected; thus, the threshold pore-throat size to determine the effectiveness of pores under ultrasonic measurement is estimated as $0.15 \mu\text{m}$. In Fig. 8, the estimated threshold pore-throat size lies around the division of the dual porosity structure, and it approximately divides the pore volume into micropore and macropore sections. While the least squares regression technique may be applied to find the optimum value of the threshold pore throat, there are only 16 eligible pore-throat sizes (corresponding to the mercury

injection pressures same for all the samples), and the hit-and-miss method we applied is convenient and sufficient to find the optimum value.

PORE GEOMETRY FROM NMR LOG

Nuclear-magnetic-resonance (NMR) log measurement is based on the strong response of hydrogen nucleus to external magnetic field (Coats *et al.* 1999). Determining pore size distribution from NMR log was first brought up by Loren and Robinson (1970). The pore size distribution can be estimated using either T_1 (longitudinal relaxation time) distribution and T_2 (transverse relaxation time) distribution. For a single spherical pore saturated with brine, T_2 is proportional to the pore size, i.e.,

$$\frac{1}{T_2} \approx \rho_2 \left(\frac{S}{V} \right) = \frac{3\rho_2}{R_{pore}}, \quad (13)$$

where ρ_2 is the T_2 surface relaxivity related to mineral properties, and S/V is the surface-to-volume ratio of the pore. The magnetization signal decays after external magnetic field is turned off, and the signal amplitude is given by (Kenyon 1989)

$$M(t) = M_0 e^{-\rho_2 \left(\frac{S}{V} \right) t}. \quad (14)$$

When the complete distribution of the 100% brine-saturated pores are considered, the overall signal can be used to estimate T_2 spectrum by calibration with measured porosity (Coats *et al.* 1999). Since the NMR T_2 spectrum is closely related to pore size distribution, it is not surprising that there is a good correlation between pore-throat distribution derived from mercury injection and NMR T_2 distribution. Overlaying

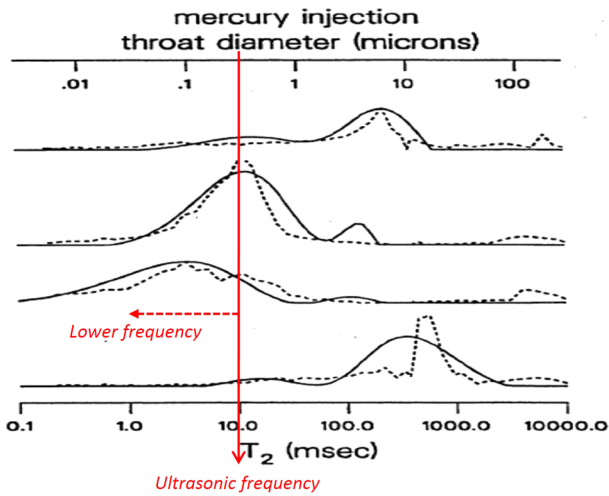


Figure 10 Correlation between MICP pore-throat diameter (dashed curve) and NMR T_2 distribution (solid curve) by overlaying two types of curves together (after Edwards 1999). The bold red arrow marks the position of the inverted threshold pore-throat diameter by matching ultrasonic data and MICP data (see Fig. 9). Therefore, the threshold T_2 is about 10 ms. The bold red arrow will move leftward for lower frequency measurement.

the NMR T_2 distribution curve with pore-throat size distribution curve derived from MICP, correlation between NMR T_2 and pore-throat size can be set up (Figure 10). In previous section we have estimated the threshold pore-throat diameter as $0.30 \mu\text{m}$. From the correlation we found that the corresponding threshold NMR T_2 is about 10 ms, which is very close to the commonly used value of 12 ms for $T_{2\text{cutoff}}$. $T_{2\text{cutoff}}$ is a threshold value for the estimation of the bulk volume of irreducible water or irreducible water saturation (Fig. 11). Thus, the irreducible water saturation can be used to approximate the effective porosity for Gassmann fluid substitution. This confirms why it is better to use effective porosity for Gassmann fluid substitution for the loose sandstone core sample from Gulf of Mexico (Fig. 4).

In the above analysis, the threshold pore-throat size or T_2 cutoff is based on inversion of ultrasonic velocity measurement. For log data and seismic data acquired at the lower frequency, the effective porosity for Gassmann fluid substitution will increase because there is more time for pore fluids in smaller pores or pores connected by narrower pore throats to reach pressure equilibrium with the pore fluids in the

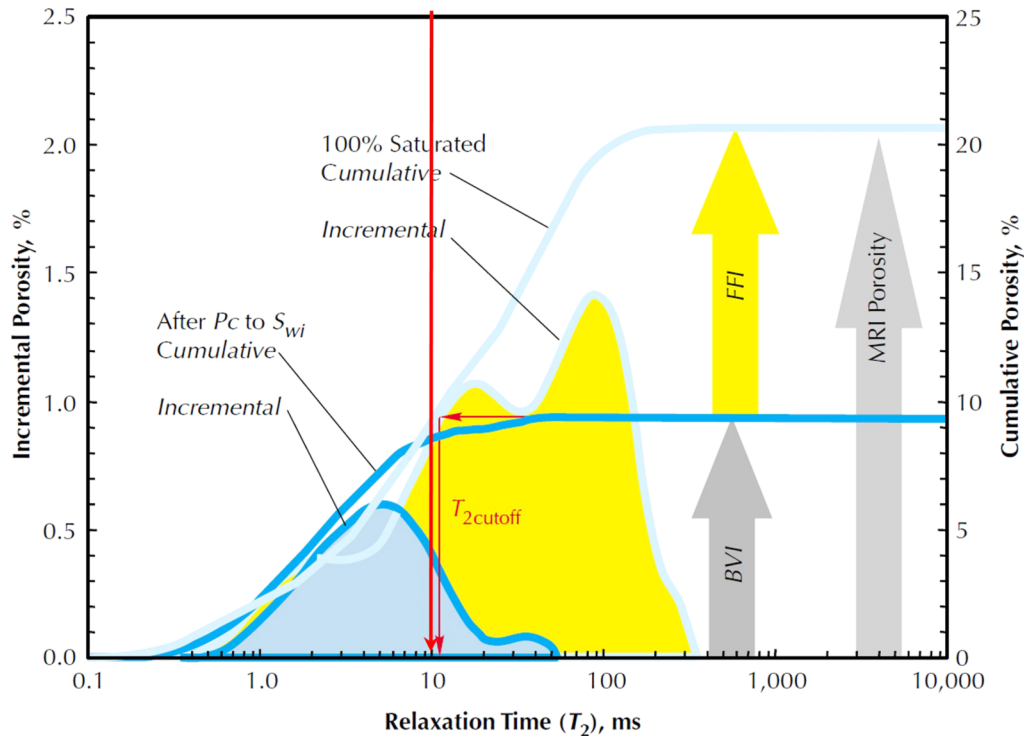


Figure 11 Comparison of threshold NMR T_2 inverted from tight gas sandstone laboratory measurement with $T_{2\text{cutoff}}$ used for estimation of irreducible water saturation. The bold red arrow marks the position of 10 ms, which is the inverted threshold NMR T_2 from estimation of dynamic effective porosity in Gassmann's equation (modified from Coates *et al.* 1999).

macropore system; therefore, the threshold pore-throat size or T_2 cutoff will decrease. The recently developed low-frequency measurement technique (Batzle, Han, and Hofmann 2006) can measure the dispersion and attenuation of acoustic waves passing through sedimentary rocks under different saturation conditions in a continuous frequency range from less than one hertz to several thousand hertz. If we have both reliable low frequency measurement and information about the pore-throat size distribution or T_2 distribution of the sample, we can invert the effective porosity from different frequency measurements and set up an empirical correlation between frequency and threshold pore-throat size or NMR T_2 . For practical application of fluid substitution on log data, if we have the NMR log, we can use the correlation between frequency and threshold T_2 to construct a log curve of effective porosity for more reliable prediction of the saturation effect.

CONCLUSIONS

Due to strong absorption by the mineral surfaces and inefficient communication with the macropore system, part of the pore fluids located on the mineral surface or in the microcracks cannot be approximated as frictionless fluids. This part of pore fluids does not satisfy the assumption of the Gassmann theory and is suggested to be accounted in the solid rock frame. Therefore, instead of the total porosity, the effective porosity should be used in Gassmann's equation for fluid substitution. Integrated study of ultrasonic laboratory measurement data, petrographic data, mercury-injection-capillary-pressure data, and nuclear magnetic resonance T_2 data confirms the rationality of using effective porosity for Gassmann fluid substitution. The effective porosity should be frequency dependent. Without information of the pore geometry, the irreducible water saturation can be used to estimate the effective porosity.

ACKNOWLEDGEMENTS

The authors would like to thank the Fluids/DHI consortium sponsors for supporting the consortium and this study, and H. Zhao for the laboratory measurements.

REFERENCES

- Bagrintseva K.I. 1977. *Carbonate Rocks: Oil and Gas Reservoirs*. Nedra, Moscow.
- Baechle G.T., Eberli G.P., Weger R.J. and Massaferro J.L. 2009. Changes in dynamic shear moduli of carbonate rocks with fluid substitution. *Geophysics* 74(3), E135–E147.
- Banin A. and Amiel A. 1970. A correlative study of the chemical and physical properties of a group of natural soils of Israel. *Geoderma* 3, 180–198.
- Batzle M.L., Han D.-H. and Hofmann R. 2006. Fluid mobility and frequency-dependent seismicity velocity—Direct measurements. *Geophysics* 71(1), N1–N9.
- Berryman J.G. 1999. Origin of Gassmann's equations. *Geophysics* 64 (5), 1627–2629.
- Berryman J.G. and Milton G.W. 1991. Exact results for generalized Gassmann's equations in composite porous media with two constituents. *Geophysics* 56(12), 1950–1960.
- Brunauer S., Emmett P.H. and Teller E. 1938. Adsorption of gases in multimolecular layers. *Journal of the American Chemical Society* 60, 309–319.
- Carcione J.M., Helle H.B., Santos J.E. and Ravazzoli C.L. 2005. A constitutive equation and generalized Gassmann modulus for multimineral porous media. *Geophysics* 70(2), N17–N26.
- Chilingarian G.V., Chang J. and Bagrintseva K.I. 1990. Empirical expression of permeability in terms of porosity, specific surface area, and residual water saturation of carbonate rocks. *Journal of Petroleum Science and Engineering* 4, 317–322.
- Ciz R. and Shapiro S.A. 2007. Generalization of Gassmann equations for porous media saturated with a solid material. *Geophysics* 72(6), A75–A79.
- Coates G.R., Xiao L. and Prammer M.G. 1999. *NMR Logging Principles and Applications*. Halliburton Energy Services Publication, Houston.
- Cook J.E., Goodwin L.B. and Boutt D.F. 2011. Systematic diagenetic changes in the grain-scale morphology and permeability of a quartz-cemented quartz arenite. *AAPG Bulletin* 95(6), 1067–1088.
- Corey A.T. 1986. *Mechanics of Immiscible Fluids in Porous Media*, 2nd Edition. Water Resource Publication.
- Davis J.M., Roy N.D., Mozley P.S. and Hall J.S. 2006. The effect of carbonate cementation on permeability heterogeneity in fluvial aquifers: an outcrop analog study. *Sedimentary Geology* 184, 267–280.
- Dillon C.G., Worden R.H. and Barclay S.A. 2004. Simulation of the effects of diagenesis on the evolution of sandstone porosity. *Journal of Sedimentary Research* 74(6), 877–888.
- Dvorkin J., Mavko G. and Gurevich B. 2007. Fluid substitution in shaly sediment using effective porosity. *Geophysics* 72(3), O1–O8.
- Edwards G.M. 1999. NMR Imaging of fluids and flow in porous media. In: *Methods in the Physics of Porous Media*, Vol. 35. Gassmann F. 1951. On elasticity of porous media. In: *Classics of Elastic Wave Theory: Society of Exploration Geophysicists* (eds J. Castagnia and C. Ecker). Tulsa, OK, USA.
- Grechka V. 2009. Fluid–solid substitution in rocks with disconnected and partially connected porosity. *Geophysics* 74(5), WB89–WB95.
- Gurevich B., Brajanovsk M., Galvin R.J., Muller T.M. and Toms-Steward J. 2009. P-wave dispersion and attenuation in fractured and porous reservoirs—poroelasticity approach. *Geophysical Prospecting* 57, 225–237.
- Han D.-H. 1986. *Effects of porosity and clay content on acoustic properties of sandstones and consolidated sediments*. PhD thesis, Stanford University.
- Han D.-H. and Batzle M.L. 2004. Gassmann's equation and fluid-saturation effects on seismic velocities. *Geophysics* 69, P398–405.

- Kenyon W.E., Howard J.J., Sezginer A., Straley C., Matteson A., Horkowitz K. *et al.* 1989. Pore-size distribution and NMR in microporous cherty sandstones. In: *30th Annual SPWLA Logging Symposium Transactions*.
- King M.S., Marsden J.R. and Dennis J.W. 2000. Biot dispersions for P- and S-wave velocities in partially and fully saturated sandstones. *Geophysical Prospecting* **48**, 1075–1089.
- Kuster G.T. and Toksöz M.N. 1974. Velocity and attenuation of seismic waves in two phase media. *Geophysics* **39**, 587–618.
- Leal L., Barbato R., Quaglia A., Porras J.C. and Lazard H. 2001. Bimodal behavior of mercury-injection capillary pressure curve and its relationship to pore geometry, rock-quality and production performance in a laminated and heterogeneous reservoir. In: *SPE Latin American and Caribbean Petroleum Engineering Conference*. Society of Petroleum Engineers.
- Lindquist W.B., Venkataraman A., Dunsmuir J. and Wong T.-F. 2000. Pore and throat size distributions measured from synchrotron X-ray tomographic images of Fontainebleau sandstones. *Journal of Geophysical Research* **105**(B9), 21509–21527.
- Loren J.D. and Robinson J.D. 1970. Relation between pore size, fluid and matrix properties and NML measurements. *Society of Petroleum Engineering Journal*, 268–278.
- Low P.F. 1961. Physical chemistry of clay-water interaction. *Advances in Agronomy* **13**, 269–327.
- Lunev I.V., Nigmatullin R.R., Zavidonov A.Y., Gusev A. and Manyurov I.R. 2001. The effect of clay morphology on water relaxation. *Technical Physics* **46**, 1473–1474.
- Mavko G. and Bandyopadhyay K. 2009. Approximate fluid substitution for vertical velocities in weakly anisotropic VTI rocks. *Geophysics* **74**(1), D1–D6.
- Mavko G. and Jizba D. 1991. Estimating grain-scale fluid effects on velocity dispersion in rocks. *Geophysics* **56**, 1940–1949.
- Mavko G., Mukerji T. and Dvorkin J. 1998. *The Rock Physics Handbook*. Cambridge University Press.
- Nadeau P.H. and Hurst A. 1991. Application of back-scattered electron microscopy to the quantification of clay mineral microporosity in sandstones. *Journal of Sedimentary Petrology* **61**(6), 921–925.
- Neasham J.W. 1977. The morphology of dispersed clay in sandstone reservoirs and its effect on sandstone shaliness, pore space and fluid flow properties. In: *Proceedings of the 52nd Annual Technical Conference*.
- Owolabi O.O. and Watson R.W. 1993. Estimating recovery efficiency and permeability from mercury capillary pressure measurements for sandstone. In: *SPE Regional Eastern Meeting*. Society of Petroleum Engineers.
- Panda M.N. and Lake L.W. 1995. A physical model of cementation and its effects on single-phase permeability. *American Association of Petroleum Geologists Bulletin* **79**, 431–443.
- Petersen L.W., Moldrup P., Jacobsen O.H. and Dolston D. 1996. Relations between specific surface area and soil physical and chemical properties. *Soil Science* **161**, 9–21.
- Pinneker E.V. 2010. *General Hydrogeology*. Cambridge University Press.
- Plaster E.J. 2008. *Soil Sciences and Management*, 5th Edition. Delmar Publishers.
- Resurreccion A.C., Moldrup P., Tuller M., Ferre T.P.A., Kawamoto K., Komatsu T. *et al.* 2011. Relationship between specific surface area and the dry end of the water retention curve for soils with varying clay and organic carbon contents. *Water Resources Research* **47**, W06522.
- Robinson K.L. and Taylor G.J. 2014. Heterogeneous distribution of water in the Moon. *Nature Geoscience* **7**, 401–408.
- Rose J.L. 1999. *Ultrasonic Waves in Solid Media*. Cambridge University Press.
- Salem H.S. and Chilingarian G.V. 1999. Determination of specific surface area and mean grain size from well-log data and their influence on physical behavior of offshore reservoirs. *Journal of Petroleum Science and Engineering* **22**, 241–252.
- Sarout J. 2012. Impact of pore space topology on permeability, cut-off frequencies and validity of wave propagation theories. *Geophysical Journal International* **189**, 481–492.
- Saxena N. and Mavko G. 2014. Exact equations for fluid and solid substitution. *Geophysics* **79**(3), I21–I32.
- Sil S., Sen M.K. and Gurevich B. 2011. Analysis of fluid substitution in a porous and fractured medium. *Geophysics* **76**(3), WA157–WA166.
- Skelton C. 2004. Fluid substitution in laminated sands. *The Leading Edge* **5**, 485–493.
- Smith T.M., Sondergeld C.H. and Rai S.R. 2003. Gassmann fluid substitution: A tutorial. *Geophysics* **68**(2), 430–440.
- Tiab D. and Donaldson E.C. 2004. *Petrophysics: Theory and Practice of Measuring Reservoir Rock and Fluid Transport Properties, 2nd Edition*. Elsevier.
- Yale L.B. (compiler) 1984. *Rock Catalog, Stanford Rock Physics, Vol. 1*. Stanford University.
- Yan F. and Han D.-H. 2011. Theoretical validation of fluid substitution by Hashin-Schtrikman bounds. 81st SEG meeting, San Antonio, USA, Expanded Abstracts.
- Yan F., Han D.-H., Yao Q. and Zhao X. 2014. Prediction of seismic wave dispersion and attenuation from ultrasonic velocity measurements. *Geophysics* **79**(5), WB1–WB8.
- Vanorio T., Scotellaro C. and Mavko G. 2007. “To fluid-substitute or not to fluid-substitute”: How pore shape and chemical processes affect Gassmann’s predictability. 77th SEG meeting, San Antonio, USA, Expanded Abstracts.
- Velasco K.K. (compiler) 1986. *Rock Catalog, Stanford Rock Physics, Vol. 3*. Stanford University.
- Wardlaw N.C. and McKellar M. 1981. Mercury porosimetry and the interpretation of pore geometry in sedimentary rocks and artificial models. *Powder Technology* **29**, 127–143.
- Wardlaw N.C., Li Y. and Forbes D. 1987. Pore-throat size correlation from capillary pressure curves. *Transport in Porous Media* **2**, 597–614.
- Washburn E.W. 1921. Note on a method of determination of determining the distribution of pore sizes in porous materials. *Proceedings of the National Academy of Sciences* **7**.
- Weisman M.C. 1984. *Geology of the Pine and northern Buckhead Mesa quadrangles, Mogollon Rim region, Central Arizona*. MS Thesis. Northern Arizona University.
- Wuddivira M.N., Robinson D.A., Lebron I., Brechet L., Atwell M., De Caires S. *et al.* 2012. Estimation of soil clay content from hygroscopic water content measurements. *Soil Science Society of America Journal* **76**(5), 1529–1535.